Methane Dry Reforming on PdZr

International Edition: DOI: 10.1002/anie.201807463
German Edition: DOI: 10.1002/ange.201807463

Zirconium-Assisted Activation of Palladium To Boost Syngas Production by Methane Dry Reforming

*Norbert Köpfle, Thomas Götsch, Matthias Grünbacher, Emilia A. Carbonio, Michael Hävecker, Axel Knop-Gericke, Lukas Schlicker, Andrew Doran, Delf Kober, Aleksander Gurlo, Simon Penner, and Bernhard Klötzer**

Abstract: *C-saturated Pd^0 nanoparticles with an extended phase boundary to ZrO_2 evolve from a Pd^0Zr^0 precatalyst under CH_4 dry reforming conditions. This highly active catalyst state fosters bifunctional action: CO_2 is efficiently activated at oxidic phase boundary sites and Pd_xC provides fast supply of C-atoms toward the latter.*

Dry reforming of methane (DRM) allows to convert climate-harming methane and carbon dioxide into useful syngas, implying its practical use for greenhouse gas abatement and CO_2 utilization.[1] Ideally, a stoichiometry of $CH_4 + CO_2 \rightarrow 2H_2 + 2CO$ is obtained. The resulting 1:1 syngas ratio is rather useful for subsequent carbonylation or hydroformylation processes.[2] If the H_2 yield can be enhanced, for example, by using membrane reactors, also the synthesis of renewable fuels may become attractive.[3] Practical problems are associated with loss of H_2 selectivity owing to the water-gas-shift equilibrium, especially at elevated pressures[4] and with irreversible coking phenomena, especially on the less-costly Ni-based catalysts.[5–8] Alternatively, a series of highly active noble metal catalysts deserve attention from a fundamental viewpoint, due to superior coking properties.[6,7,9,10] Empirical attempts to impart this coking resistance to nickel without sacrificing activity led to a series of promising bimetallic catalysts, with $NiPd/ZrO_2$ representing one of the best.[11] Yet, the mechanistic effects of noble metal alloying of Ni are not clear. Besides potential ensemble and electronic structure effects at the bimetallic surface[12,13] different levels of metal oxide bifunctionality have been proposed, depending on the intrinsic activity of the respective pure metal component.[10] Pure Ni surfaces are in principle capable of activating both CH_4 and CO_2,[13–15] and thus a minor co-catalytic role of the support can be anticipated. In contrast, a high degree of bifunctionality can be expected, if a very good CH_4 activator such as Pd exhibits comparatively poor CO_2 activation properties.[10,15,16] Consequently, only the promotion of CO_2 activation and subsequent CO product formation at both active and abundant oxide support: Pd interface sites can establish high DRM activity. In such cases, empirical development of catalyst preparation and catalyst activation must logically aim in a particularly large (bi)metal interface to an oxidic support with good CO_2 activation kinetics. Critical parameters determining the latter encompass surface reducibility, basicity, reactivity of oxygen vacancies toward CO_2, and so on.[17]

Metal-wise, both fast supply of reactive carbon toward and high abundance at the metal oxide phase boundary (abbreviated as PB in the following) is mandatory. Pd exhibits excellent subsurface and bulk carbon diffusion and storage properties, which is not only important for a variety of catalytic applications[18] but also for graphene and carbon nanotube growth[18,19] and novel (electro)catalytic applications of graphene-covered Pd nanostructures.[20] Thus, the experimental and theoretical investigation of carbon resegregation and reactivity on Pd is a topic of general interest.[21,22]

Owing to their structural heterogeneity and the limited applicability of surface-sensitive in situ spectroscopy techniques such as AP-XPS, technical powder catalysts usually do not allow to extract unambiguous evidence for the catalytic role of the PB. The use of conductive (bi)metallic substrates, on which a thin active layer forms under reaction conditions by oxidative segregation, both allows the circumvention of conductivity problems and provides a quasi-2D region of spectral observation. Thus, both a surface and bulk bimetallic PdZr model catalyst approach toward active PB sites was employed. The initial and DRM-induced states of these model systems are represented in the Supporting Informa-

[*] M. Sc. N. Köpfle, M. Sc. T. Götsch, M. Sc. M. Grünbacher, Priv.-Doz. Dr. S. Penner, Prof. B. Klötzer
Institute of Physical Chemistry, University of Innsbruck
Innrain 52 c, 6020 Innsbruck (Austria)
E-mail: Bernhard.Kloetzer@uibk.ac.at

Dr. E. A. Carbonio, Dr. M. Hävecker, Dr. A. Knop-Gericke
Department of Inorganic Chemistry
Fritz-Haber-Institute of the Max-Planck-Society
Faradayweg 4–6, 14195 Berlin (Germany)

Dr. E. A. Carbonio
Helmholtz-Zentrum Berlin für Materialien und Energie GmbH, BESSY II
Albert-Einstein-Straße 15, 12489 Berlin (Germany)

Dipl.-Ing. L. Schlicker, Dipl.-Ing. D. Kober, Prof. A. Gurlo
Fachgebiet Keramische Werkstoffe, Institut für Werkstoffwissenschaften und -technologien, Technische Universität Berlin
Hardenbergstr. 40, 10623 Berlin (Germany)

A. Doran
Advanced Light Source, Beamline 12.2.2.
Lawrence Berkeley National Laboratory
Berkeley, CA 94720 (USA)

Supporting information and the ORCID identification number(s) for the author(s) of this article can be found under: https://doi.org/10.1002/anie.201807463.

© 2018 The Authors. Published by Wiley-VCH Verlag GmbH & Co. KGaA. This is an open access article under the terms of the Creative Commons Attribution License, which permits use, distribution and reproduction in any medium, provided the original work is properly cited.

tion, Figure S1. A CVD-prepared Zr^0 subsurface alloy state on Pd foil showed oxidative segregation of ZrO_xH_y domains at the Pd surface under DRM conditions, thus forming an inverse ZrO_xH_y island on bulk Pd model catalyst, which showed to be somewhat more active than its individual components ZrO_2 and Pd.[23] Alternatively, the in situ activation of bulk intermetallic precursors is a particularly efficient way to generate a large amount of PB sites between (bi)metallic and oxidic nanoparticles, as shown in the lower part of the Supporting Information, Figure S1.[24] Both approaches were followed in this work, using a combination of synchrotron-based XRD and XPS analysis under DRM conditions to characterize both the bulk-related phase changes and the active surface/interface state in situ.

Details of sample preparation of the bulk-intermetallic and sub-surface alloy Pd^0Zr^0 samples are given in the Experimental Section of the Supporting Information and in previous reports.[23,25] The partially oxidized pre-reaction surface state on top of the bulk-intermetallic substrate was characterised by XPS (Supporting Information, Figure S2). To characterize the bulk composition of the precatalyst versus the DRM operando state, in situ XRD spectra were taken before and during reaction. The corresponding effects are shown in Figure 1. The relevant 2θ range of the integrated data can be accordingly seen in (a). Half of the recorded detector image, including the phase assignment, is displayed in (b).

The initial sample contains Pd_2Zr and Pd_3Zr and is coarse crystalline, as can be derived from the spotty, that is, not completely continuous, rings. Under DRM conditions, metallic and crystalline Pd is formed, as well as tetragonal ZrO_2. At the same time, the fraction of Pd_2Zr and Pd_3Zr in the phase mixture decreases, inferred from the significantly lower intensities of the associated reflexes compared to the initial sample. Both newly formed phases, namely Pd and tetragonal (t-)ZrO_2, appear as completely continuous rings in the detector image and therefore, have a fine or nanocrystalline morphology. Both the crystallite size and the lattice constant of Pd^0 can be estimated via Rietveld analysis, yielding a value of 3.914 Å and a mean crystallite size of about 7.5 nm during DRM at 800 °C. As will be shown in the context of Figure 3, in situ XPS clearly revealed a C_{bulk} loaded carbidic state of Pd^0 under DRM conditions. Accordingly, a pronounced lowering of the Pd^0 lattice parameter is observed (Supporting Information, Figure S3) that is due to O_2-induced C_{bulk} depletion just at the onset of partial Pd oxidation (3.898 Å, 10.3 nm mean crystallite size).

Quantitative temperature-programmed DRM reaction studies on both the subsurface and bulk intermetallic precatalysts were performed in our UHV-compatible recirculating batch reactor (for details, see the Supporting Information, Experimental Section), and compared to the activities of clean Pd metal foil and a fully ZrO_2 covered Zr foil. The bulk-intermetallic rate data are shown in Figure 2, revealing a strong, 33-fold DRM rate promotion relative to a single-phase ZrO_2 oxide film. Pure Pd foil shows hardly any measurable activity. At about 860 K the CO formation rate starts to increase exponentially with the temperature and exhibits a maximum upon reaching the final temperature of

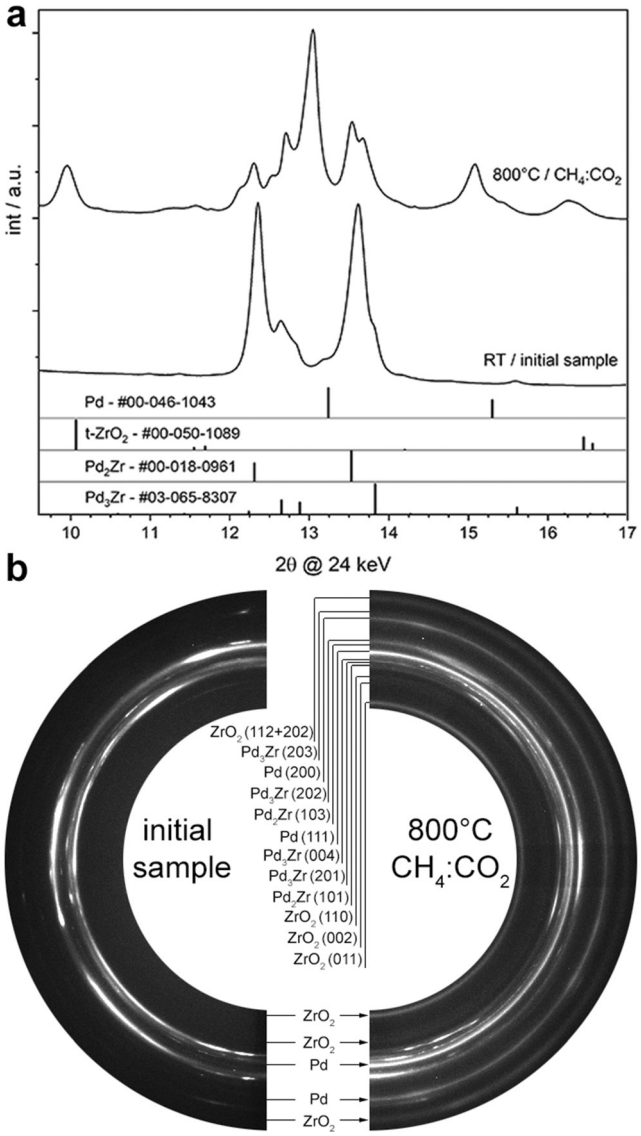

Figure 1. In situ XRD of the bulk-intermetallic Pd_xZr_y catalyst at ca. 20 °C and during DRM at 800 °C. A gas flow of 2 mL min^{-1} of CH_4/CO_2 (ratio 1:1) at ambient pressure with a heating rate of 20 K min^{-1} was applied. Initial state at room temperature: a), bottom spectrum and b), left side; in situ DRM state: a), top spectrum and b), right side.

1073 K. The subsequent isothermal rate decrease is caused by progressive reactant consumption (CH_4 and CO_2 conversion after 45 min: ca. 96 %). We note that the CO:H_2 product ratio was close to 1:1 and accordingly, the ratio of the CO_2 consumption vs. CO formation rates close to 1:2.

The complementary DRM rate data on the PdZr subsurface alloy precatalyst are plotted in the Supporting Information, Figure S4, showing only slightly higher average rates than on pure ZrO_2.

The DRM activity is effectively not scalable with the Pd^0/Zr(ox) interface sites forming in situ under DRM conditions on bulk Pd^0 (for details, see the Supporting Information, Figure S4). Rather, it is synergistically boosted by the combination of an extended PB with nanoparticulate Pd^0. The XRD results of Figure 1 show that the PB forms in situ by

 © 2018 The Authors. Published by Wiley-VCH Verlag GmbH & Co. KGaA, Weinheim

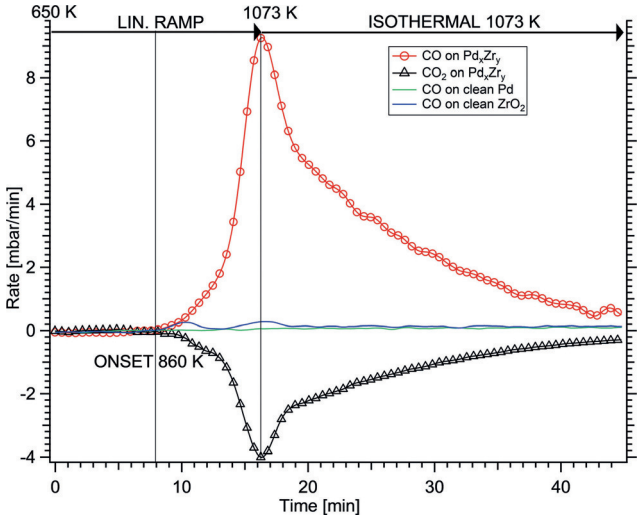

Figure 2. Temperature-programmed DRM rate profile on the Pd_xZr_y bulk-intermetallic precatalyst, plotted versus the rates measured on clean Pd foil and clean ZrO_2. Reaction conditions: 50 mbar CH_4, 50 mbar CO_2, 977 mbar He; linear temperature ramp (25 K min^{-1}) up to 1073 K, followed by isothermal reaction for 30 min.

oxidative t-ZrO_2 segregation from Pd^0Zr^0 in the DRM gas phase, and that this process provides Pd^0 in a nanodispersed form. The related C 1s core-level spectra obtained by AP-XPS on the bulk PdZr precatalyst are shown in Figure 3. They provide clear indications of considerable C_{bulk} concentrations within Pd, but only in the presence of CH_4 gas. The C 1s component at a BE of 283.0 eV (upper panel, green), as well as the Pd 3d component at 335.6 eV (lower panel, green) correspond well to literature-reported values of 335.6 eV and 282.9 eV for Pd modified by bulk-dissolved carbidic/interstitial C[22,26] and are obviously linked to ongoing C supply via the gas phase. The bulk character of this species is supported by its response to a change of the photon energy/C 1s kinetic energy, as shown in the Supporting Information, Figure S5. Upon extending the probe depth, its relative intensity to the surface-graphitic component increases. As soon as the CH_4 supply is switched off, the C_{bulk} signal disappears immediately, whereas the $C_{graphite}$ component decreases at a slower rate. Obviously, C_{bulk} is much more reactive than $C_{graphite}$ with respect to the carbon clean-off reaction in pure CO_2. The $C_{graphite}$ intensity decreases even more slowly below the level shown in Figure 3 for pure CO_2, which can be explained by a certain amount of even less reactive carbon resulting from ambient exposure prior to catalysis (for details, see the Supporting Information, Figure S6).

The related C 1s and Pd 3d spectra on the initial Pd/Zr^0 subsurface alloy exhibit no such carbidic/interstitial C_{bulk} component under otherwise identical DRM conditions(Supporting Information, Figure S7). The fundamental difference between the two model systems regards the dimensions of the respective Pd bulk. In case of the initial subsurface alloy, the in situ formed ZrO_xH_y domains reside on a practically infinite Pd bulk, which will permanently lose C_{bulk} by diffusion into deeper regions, and thus will require a very long time to reach

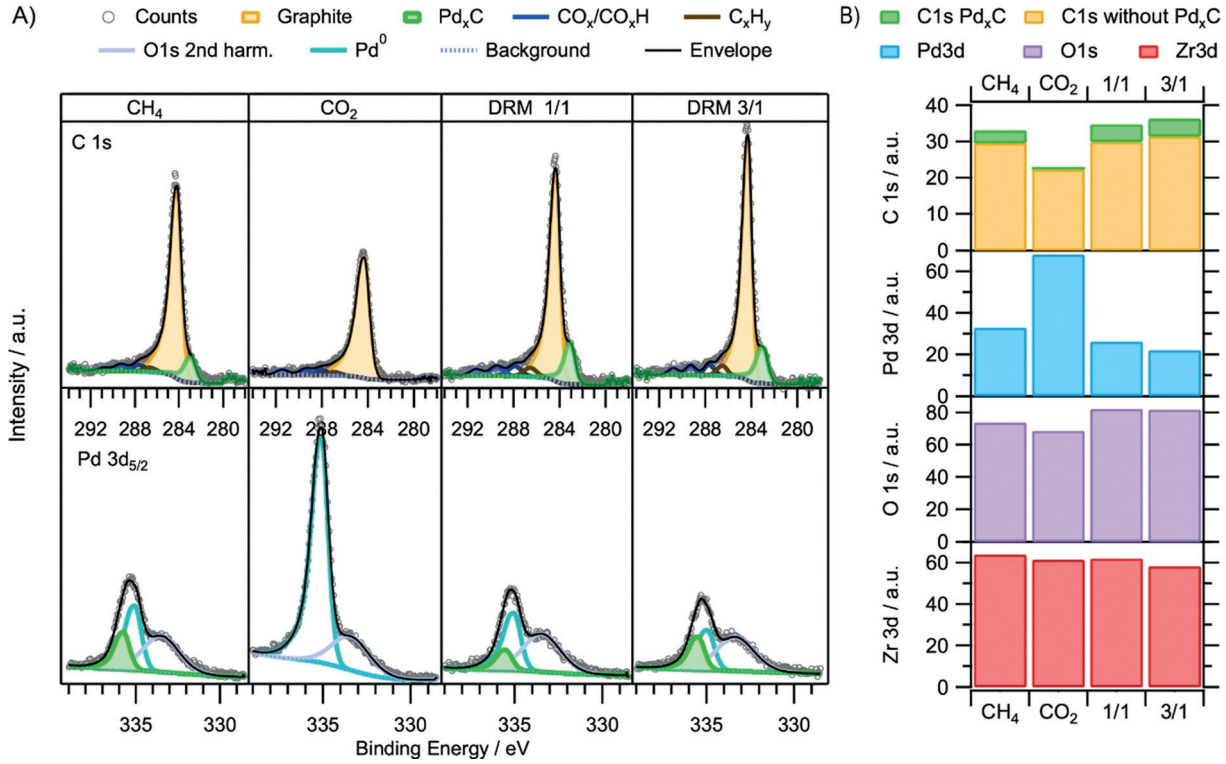

Figure 3. C 1s and Pd $3d_{5/2}$ AP-XPS spectra recorded at a common kinetic energy of 400 eV in situ during DRM at ca. 700 °C, starting from the bulk Pd_xZr_y precursor. Applied gas pressures from left to right: 0.3 mbar CH_4, 0.3 mbar CO_2, DRM 1:1 = 0.15 mbar CH_4 + 0.15 mbar CO_2, DRM 3:1 = 0.225 mbar CH_4 + 0.125 mbar CO_2. A) Corresponding C 1s and Pd $3d_{5/2}$ peak deconvolution; B) XPS intensity bar graph of the integrated C 1s, Pd 3d, O 1s, and Zr 3d regions.

 © 2018 The Authors. Published by Wiley-VCH Verlag GmbH & Co. KGaA, Weinheim

C-saturation. In contrast, the bulk intermetallic decomposes toward Pd nanoparticles in close contact to t-ZrO_2 domains. The reduced Pd bulk dimensions obviously facilitate/accelerate the accumulation of interstitially dissolved C_{bulk}.

As a consequence, carbon resegregation from sufficiently C-supersaturated Pd regions will enhance the surface-near C_{ads} concentration and, in due course, the nucleation/growth of graphene/graphite domains.[27] In the same turn, an enhanced rate of C bulk and surface diffusion toward the PB must result. From the combination of the extended PB and the reduced Pd metal dimensions, the much higher reaction rates on the bulk intermetallic precursor can be rationalized. Still, the exact spatial distribution of the ZrO_2, graphitic, and Pd_xC domains remains to be clarified under analogous DRM conditions, for example by using in situ HRTEM techniques.

On both model systems, the $C_{graphite}$ species exhibit a dynamic and reversible response both to changes of the gas phase composition and of the temperature. On the bulk intermetallic system, the $C_{graphite}$ species reacted much more slowly than the C_{bulk} species. We observed on both model systems that the $C_{graphite}$ intensities (and on the initial bulk intermetallic also the C_{bulk} intensities) reached a steady-state value after establishing constant partial pressure and temperature conditions. These steady state values are depicted on the right sides of Figure 3 (bulk intermetallic precursor) and the Supporting Information, Figure S7 (subsurface Zr^0), together with the related final Zr 3d, O 1s, and Pd 3d intensities. From the relative intensity changes in Figure 3, a preferential accumulation of carbon on the Pd particles can be deduced, as increasing methane partial pressures lead to a dominant screening of the Pd 3d signal. In turn, the oxide surface-related Zr 3d and O 1s intensities rather show a weak or even opposite response. This behavior is in strong contrast to the intensity trends observed on the initial subsurface-Zr^0 system, where preferential screening of the Zr 3d and O 1s signals is observed upon C accumulation. Again we suggest that, despite of continuous C supply via CH_4(g) to Pd, the quasi-infinite dimensions of the Pd foil allow for permanent C loss to deeper bulk regions, causing little C-supersaturation in surface-near regions and thus no or heavily delayed graphite nucleation/growth. Especially under the influence of the highly intense and ionizing synchrotron X-ray beam, C accumulation on top of the oxidatively segregated ZrO_x domains is thus preferred. Moreover, C-diffusion through the surface-ZrO_x domains is expected to be hardly possible or at least kinetically strongly retarded. The combination of these effects can eventually explain the observed preferential C-accumulation on the oxidic domains. This carbon can be reacted off quantitatively in pure CO_2, likely because of intrinsically close vicinity to the active PB.

By increasing the temperature, the clean-off reaction rate at the PB of the initial PdZr bulk model is enhanced, and above 700 °C a lowering of the steady-state C 1s signal results, as shown in the Supporting Information, Figure S8. This is likely due to a changed balance of graphitic C formation and redissolution rates. This effect could also imply a possible mechanistic explanation for the intermediate temperature coking region[28] of DRM, which can be interpreted by a shift of the Boudouard equilibrium toward carbon. Assuming a faster increase of the C clean-off rate at the PB with temperature in comparison to the net rate of partially reversible graphene/graphite accumulation, the inverse Boudouard process $C + CO_2 \rightarrow 2\,CO$ at the PB will simply overtake the net $C_{graphite}$ deposition rate at sufficiently high temperatures.

In conclusion, the surface-near regions of the bulk PdZr pre-catalyst are oxidatively decomposed under realistic DRM conditions and the resulting Pd^0 nanoparticles provide an appropriate near-surface carbon loading at the resulting Pd^0/t-ZrO_2 interface at about 700 °C, as depicted in Scheme 1. This, in turn, creates optimized conditions for bifunctional catalyst operation: Pd^0 regions favor fast supply of reactive C-atoms toward the phase boundary, whereas Zr(ox) sites[10,16] assist in CO_2 activation and the transfer of CO_2-derived oxygen to the latter, thus providing optimum conditions for high CO-activity.

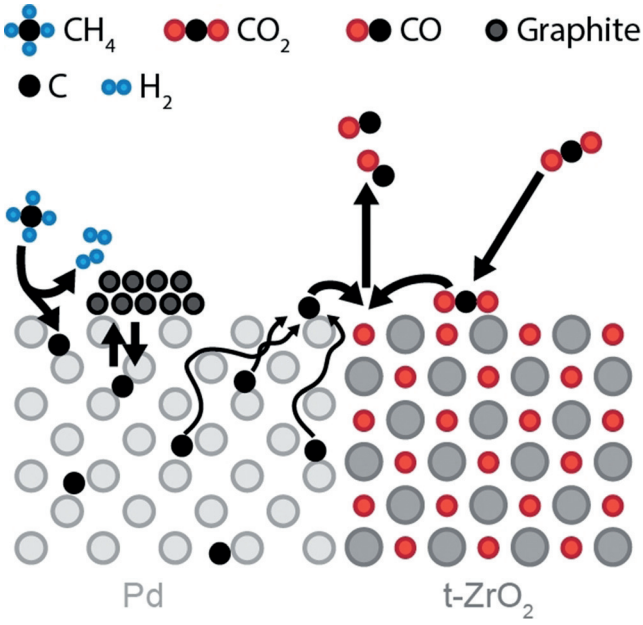

Scheme 1. Proposed DRM mechanism leading to enhanced CO formation at the Pd/t-ZrO_2 interface.

Empirical attempts to control coking of, for example, Ni by specifically active supports such as $CeZrO_x$[5,29] seem to make use of this principle. Faster C-depletion of the metallic component via an accelerated phase boundary reaction can directly lower the C concentration of the metal particles and thus initially disfavor nucleation and growth of graphite-type C-species, but also enhance the relative amount of redissolution of the latter in the metal as C_{bulk} under stationary reaction conditions. This scenario provides a solid basis for directional promotion of microkinetic steps leading both to enhanced activity and improved control of carbon chemistry during DRM. Important implications for knowledge-based DRM catalyst synthesis, at least if C-dissolving metals such as Ni and Pd are involved, are: 1) optimization of phase boundary dimensions and CO_2 activation properties of the

 © 2018 The Authors. Published by Wiley-VCH Verlag GmbH & Co. KGaA, Weinheim

support; 2) adjustment of (bi)metal particle size to achieve C_{bulk} depletion even in metallic regions with the largest distance to the phase boundary; 3) use of (bi)metallic catalysts with suppressed nucleation- and growth kinetics of graphite-type C-species, at least within the DRM temperature range; and 4) high abundance and reactivity of interfacial C_{ads} species, achievable via optimized CH_4 adsorption/sticking at the metallic surface and fast bulk/surface diffusion to not too strongly C-binding sites at or close to the PB. As shown in this work, the use of intermetallic precursors such as Pd_xZr_y is one way to match these criteria.

As a perspective for future research, the detailed reaction mechanism of CO_2 splitting toward reactive oxygen-, carbonate- and/or formate-type species[17,30] at the PB remains to be clarified. Distinct oxygenate intermediates were observed in this study by AP-XPS (Figure 3; Supporting Information, Figures S2, S5, S7), which appear to reside at the PB or the oxidic surface, and which exhibit a partially reversible dynamic response to gas-phase- and temperature changes. In the context of oxygenated C1 species, support acidity vs. basicity has been proposed to influence their specific type and distribution at the PB.[31] In principle, CO_2 splitting via reactive vacancies at the PB can proceed directly or via intermediate vacancy-bonded oxygenates.[32,33] Clearly, the observed oxygenate C 1s species deserve future experimental and theoretical attention, as the poor data quality and ambiguous background correction in the region above about 286 eV did not allow the assignment of any of the species safely or the distinguishing of in situ gas-phase induced intensity trends from other background effects without doubt.

(Bi)metal-wise, further fundamental work should aim in directional promotion of C_{ads} reactivity via electronic modulation of, for example, C bond strength[34] in combination with lowered barriers for C_{bulk} diffusion and redissolution of $C_{graphite}$, to enhance the PB-abundance of reactive C atoms.

Acknowledgements

This work was financially supported by the Austrian Science Fund through grant F4503-N16. N.K. acknowledges a PhD position via doctoral programme "reactivity and catalysis" of the University of Innsbruck. The authors thank the HZB/BESSY II staff for their support of the in situ XPS measurements at beamline ISISS-PGM. Financial support by the project CALIPSOplus under the Grant Agreement 730872 from the EU Framework Programme for Research and Innovation HORIZON 2020 is acknowledged. This research used resources of the Advanced Light Source, which is a DOE Office of Science User Facility under contract no. DE-AC02-05CH11231. L.S. acknowledges the funding of his work by an ALS doctoral fellowship.

Conflict of interest

The authors declare no conflict of interest.

Keywords: CO_2 activation · heterogeneous catalysis · methane dry reforming · photoelectron spectroscopy · X-ray diffraction

How to cite: *Angew. Chem. Int. Ed.* **2018**, *57*, 14613–14618
Angew. Chem. **2018**, *130*, 14823–14828

[1] S. Afzal, D. Sengupta, A. Sarkar, M. El-Halwagi, N. Elbashir, *ACS Sustainable Chem. Eng.* **2018**, *6*, 7532.
[2] a) E. C. Alyea, D. He, J. Wang, *Appl. Catal. A* **1993**, *104*, 77; b) S. Wang, G. Q. Lu, G. J. Millar, *Energy Fuels* **1996**, *10*, 896; c) S. A. Ghoneim, R. A. El-Salamony, S. A. El-Temtamy, *WJET* **2016**, *04*, 116.
[3] a) E. R. Minardi, S. Chakraborty, S. Curcio in *Membrane Reactors for Energy Applications and Basic Chemical Production*, Elsevier, Amsterdam, **2015**, pp. 99–144; b) M. L. Bosko, J. F. Múnera, E. A. Lombardo, L. M. Cornaglia, *J. Membr. Sci.* **2010**, *364*, 17.
[4] S. T. Oyama, P. Hacarlioglu, Y. Gu, D. Lee, *Int. J. Hydrogen Energy* **2012**, *37*, 10444.
[5] A. Wolfbeisser, O. Sophiphun, J. Bernardi, J. Wittayakun, K. Föttinger, G. Rupprechter, *Catal. Today* **2016**, *277*, 234.
[6] A. T. Ashcroft, A. K. Cheetham, M. L. H. Green, P. D. F. Vernon, *Nature* **1991**, *352*, 225.
[7] J. R. Rostrup-Nielsen, *J. Catal.* **1993**, *144*, 38.
[8] M. C. J. Bradford, M. A. Vannice, *Appl. Catal. A* **1996**, *142*, 73.
[9] a) Y. Sakai, H. Saito, T. Sodesawa, F. Nozaki, *React. Kinet. Catal. Lett.* **1984**, *24*, 253; b) P. Ferreira-Aparicio, C. Márquez-Alvarez, I. Rodríguez-Ramos, Y. Schuurman, A. Guerrero-Ruiz, C. Mirodatos, *J. Catal.* **1999**, *184*, 202; c) J. Kehres, J. G. Jakobsen, J. W. Andreasen, J. B. Wagner, H. Liu, A. Molenbroek, J. Sehested, I. Chorkendorff, T. Vegge, *J. Phys. Chem. C* **2012**, *116*, 21407; d) F. Solymosi, G. Kutsán, A. Erdöhelyi, *Catal. Lett.* **1991**, *11*, 149; e) Y. Zhao, Y.-X. Pan, Y. Xie, C.-j. Liu, *Catal. Commun.* **2008**, *9*, 1558; f) C. Rameshan, H. Li, K. Anic, M. Roiaz, V. Pramhaas, R. Rameshan, R. Blume, M. Hävecker, J. Knudsen, A. Knop-Gericke, et al., *J. Phys.: Condens. Matter* **2018**, *30*, 264007.
[10] J. H. Bitter, K. Seshan, J. A. Lercher, *J. Catal.* **1998**, *176*, 93.
[11] B. Steinhauer, M. R. Kasireddy, J. Radnik, A. Martin, *Appl. Catal. A* **2009**, *366*, 333.
[12] a) D. Pakhare, J. Spivey, *Chem. Soc. Rev.* **2014**, *43*, 7813; b) P. Strasser, S. Koh, T. Anniyev, J. Greeley, K. More, C. Yu, Z. Liu, S. Kaya, D. Nordlund, H. Ogasawara, et al., *Nat. Chem.* **2010**, *2*, 454; c) P. Liu, J. K. Nørskov, *Phys. Chem. Chem. Phys.* **2001**, *3*, 3814; d) F. Gao, D. W. Goodman, *Chem. Soc. Rev.* **2012**, *41*, 8009.
[13] J. Zhang, H. Wang, A. Dalai, *J. Catal.* **2007**, *249*, 300.
[14] a) J. Wei, E. Iglesia, *J. Catal.* **2004**, *224*, 370; b) M. C. J. Bradford, M. A. Vannice, *Catal. Rev. Sci. Eng.* **1999**, *41*, 1.
[15] L. Foppa, T. Margossian, S. M. Kim, C. Müller, C. Copéret, K. Larmier, A. Comas-Vives, *J. Am. Chem. Soc.* **2017**, *139*, 17128.
[16] J. H. Bitter, K. Seshan, J. A. Lercher, *J. Catal.* **1997**, *171*, 279.
[17] M.-S. Fan, A. Z. Abdullah, S. Bhatia, *ChemCatChem* **2009**, *1*, 192.
[18] C. Barth, *J. Phys. Chem. C* **2018**, *122*, 522.
[19] R. A. Segura, S. Hevia, P. Häberle, *J. Nanosci. Nanotechnol.* **2011**, *11*, 10036.
[20] a) Q. Fu, X. Bao, *Chem. Soc. Rev.* **2017**, *46*, 1842; b) D. Deng, K. S. Novoselov, Q. Fu, N. Zheng, Z. Tian, X. Bao, *Nat. Nanotechnol.* **2016**, *11*, 218.
[21] H. S. Mok, A. Ebnonnasir, Y. Murata, S. Nie, K. F. McCarty, C. V. Ciobanu, S. Kodambaka, *Appl. Phys. Lett.* **2014**, *104*, 101606.
[22] O. Balmes, A. Resta, D. Wermeille, R. Felici, M. E. Messing, K. Deppert, Z. Liu, M. E. Grass, H. Bluhm, R. van Rijn, et al., *Phys. Chem. Chem. Phys.* **2012**, *14*, 4796.

 © 2018 The Authors. Published by Wiley-VCH Verlag GmbH & Co. KGaA, Weinheim

[23] N. Köpfle, L. Mayr, P. Lackner, M. Schmid, D. Schmidmair, T. Götsch, S. Penner, B. Kloetzer, *ECS Trans.* **2017**, *78*, 2419.
[24] L. Mayr, B. Klötzer, D. Schmidmair, N. Köpfle, J. Bernardi, S. Schwarz, M. Armbrüster, S. Penner, *ChemCatChem* **2016**, *8*, 1778.
[25] L. Mayr, X.-R. Shi, N. Köpfle, C. A. Milligan, D. Y. Zemlyanov, A. Knop-Gericke, M. Hävecker, B. Klötzer, S. Penner, *Phys. Chem. Chem. Phys.* **2016**, *18*, 31586.
[26] a) D. Teschner, J. Borsodi, A. Wootsch, Z. Révay, M. Hävecker, A. Knop-Gericke, S. D. Jackson, R. Schlögl, *Science* **2008**, *320*, 86; b) B. S. Ahn, S. G. Jeon, H. Lee, K. Y. Park, Y. G. Shul, *Appl. Catal. A* **2000**, *193*, 87.
[27] R. Rameshan, V. Vonk, D. Franz, J. Drnec, S. Penner, A. Garhofer, F. Mittendorfer, A. Stierle, B. Klötzer, *Sci. Rep.* **2018**, *8*, 2662.
[28] a) A. W. Budiman, S.-H. Song, T.-S. Chang, C.-H. Shin, M.-J. Choi, *Catal. Surv. Asia* **2012**, *16*, 183; b) A. M. Gadalla, B. Bower, *Chem. Eng. Sci.* **1988**, *43*, 3049.
[29] a) S. Damyanova, B. Pawelec, K. Arishtirova, M. M. Huerta, J. L. G. Fierro, *Appl. Catal. B* **2009**, *89*, 149; b) M. M. Makri, M. A. Vasiliades, K. C. Petallidou, A. M. Efstathiou, *Catal. Today* **2016**, *259*, 150.
[30] M. Kogler, E.-M. Köck, B. Klötzer, L. Perfler, S. Penner, *J. Phys. Chem. C* **2016**, *120*, 3882.
[31] M. Simonov, V. Rogov, M. Smirnova, V. Sadykov, *Catalysts* **2017**, *7*, 268.
[32] A. K. Opitz, A. Nenning, C. Rameshan, M. Kubicek, T. Götsch, R. Blume, M. Hävecker, A. Knop-Gericke, G. Rupprechter, B. Klötzer, et al., *ACS Appl. Mater. Interfaces* **2017**, *9*, 35847.
[33] M. Grünbacher, T. Götsch, A. K. Opitz, B. Klötzer, S. Penner, *ChemPhysChem* **2018**, *19*, 93.
[34] L. Foppa, M.-C. Silaghi, K. Larmier, A. Comas-Vives, *J. Catal.* **2016**, *343*, 196.

Manuscript received: June 28, 2018
Accepted manuscript online: September 4, 2018
Version of record online: September 17, 2018

 © 2018 The Authors. Published by Wiley-VCH Verlag GmbH & Co. KGaA, Weinheim